Applied Catalysis B: Environmental 245 (2019) 122–129

Contents lists available at ScienceDirect

Applied Catalysis B: Environmental

journal homepage: www.elsevier.com/locate/apcatb

Chimney effect of the interface in metal oxide/metal composite catalysts on the hydrogen evolution reaction

Lishan Peng, Xingqun Zheng, Li Li*, Ling Zhang, Na Yang, Kun Xiong, Hongmei Chen, Jing Li, Zidong Wei*

The State Key Laboratory of Power Transmission Equipment & System Security and New Technology, Chongqing Key Laboratory of Chemical Process for Clean Energy and Resource Utilization, School of Chemistry and Chemical Engineering, Chongqing University, Chongqing, 400044, China

ARTICLE INFO

Keywords:
Hydrogen evolution reaction
Heterogeneous catalysts
Interface
DFT calculation
Hydrogen binding energy

ABSTRACT

Precise atomic-level control of composition and geometric structure at the interface between two catalyst components can effectively tune the catalytic properties. Herein, we found a "chimney effect" formed on the interface between the metal oxide and Nickel metal for the hydrogen evolution reaction, using density functional theory calculations and experimental methods. This special chemical environment around the interface leads the neighboring sites to be immune to the H_2O* and OH* adsorption and to only selectively adsorb H* properly. Meanwhile, it is also beneficial for the smooth adsorption of the reactant (H*) on the interface and the easy desorption of the product (H_2) from the catalyst surface (ΔG_{H^*} close to zero). This phenomenon appears similar to a chimney of hydrogen evolution around the metal oxide/metal interface. Such "chimney effect" is a result of the interfacial charge transfer between the metal and metal oxide, and should be the nature of the interface-induced synergistic effect in metal oxide/metal composite catalysts for HER. Experiments further confirm that the catalytic activity of metal oxide/metal composites for HER can be enhanced by increasing the amount of the chimney - the interfacial metal atoms.

1. Introduction

Hydrogen is frequently promoted as an alternative energy carrier of the future due to its high energy density and the zero environmental impact of its combustion product [1–5]. The electrochemical splitting of water into hydrogen and oxygen in an electrolyzer is an effective way of producing high-purity hydrogen. To achieve efficient hydrogen production, it is necessary to employ low-cost and high-performance electrocatalysts [3,6–11].

Metal oxide/metal composite catalysts attract more and more attention due to its low-cost and comparable catalytic activity to commercial Pt/C catalysts for HER in alkaline solution [12–18]. The enhanced activity of the composite catalysts are mainly attributed to the synergistic effect between the metal oxide and metal. Many research groups devote to uncover the underlying mechanism of synergistic effect in composite catalysts for HER [19–25]. Strmcnik et al. [20,26] attributed the improved activity of metal oxide/metal catalysts to the effect of the metal oxide, because the cluster plays a reactive role in the dissociation of the water and production of the hydrogen intermediates, thus enhancing the HER kinetics. Then, they inferred that the dissociation of H_2O is an important step for HER in alkaline condition. While, Durst's team [27] claimed that OH^- adsorption or the H_2O dissociation is not the rate determining step in basic conditions, and it is the H-binding energy (HBE) that is the relevant descriptor. This conclusion was supported by Yan and co-workers [28,29]. They deduced that the OH species do not participate directly in the HER reaction through adsorption and that the HBE is the sole descriptor for the HER activity on single-metallic Pt. Therefore, the mechanism underlying the high catalytic activity of metal oxide/metal composite catalysts for the HER become more ambiguous. And the nature of the synergistic effect between the metal oxide and metal is also confusing.

In addition, many experiments have been found that the metallic nanoparticles decorated on metal oxides play the critical role in the advanced HER performance of the catalysts [30–35]. The intimate contact and the promoted electron interaction between the metal and metal oxides might improve the intrinsic catalytic activity and enhance the utilization of the catalysts. Recently, Wang Yong's team [33] found that the Ni° on the interface of Ni/NiO is critical to the outstanding catalytic activity. Our previous study [36] also found that the charge transfer between the nonmetallic atom and metal is one of the keys to

* Corresponding authors.
E-mail addresses: liliracial@cqu.edu.cn (L. Li), zdwei@cqu.edu.cn (Z. Wei).

https://doi.org/10.1016/j.apcatb.2018.12.035
Received 25 August 2018; Received in revised form 7 December 2018; Accepted 14 December 2018
Available online 15 December 2018
0926-3373/

modulate the HER activity. Among all investigated nonmetallic atoms, the O, S and Se atoms can enhance the HER activity of neighboring Ni atoms effectively. Thus, the interface between the metal oxide and metal should be vital to the HER activity. In other words, the interface-induced synergistic effect between two different catalytic components is the origin of the improving catalytic activity. Considering that not all surface sites, such as metal and metal oxides, of a composite catalyst have the same effect on the enhanced activity, identifying the active sites with the most important role and revealing the underlying mechanisms are the key task for the rational design of better metal oxide/metal composite catalysts.

Herein, we focus on studying the role of the interface between the metal oxide and metal in improving HER catalytic activity, and exploring the essential cause of the interface-induced synergistic effect for HER, using theoretical calculations and experiments. The RuO_2/Ni (001) and NiO/Ni (001) as two typical models were studied. The interfacial Ni atoms in RuO_2/Ni (001) and NiO/Ni (001) as the interface-induced optimal active sites exhibit a significant difference in electronic structure and adsorption/desorption characteristics, and form a "chimney effect" for HER. The proposed "chimney effect" shed light on the nature of the interface-induced synergistic effect, could help us understanding the enhancing catalytic activity of the metal oxide/metal composites more thoroughly and can also guide the synthesis of more effective metal oxide/metal HER catalysts.

2. Computational and experiment details

2.1. Model and computation detail

The calculations were carried out using the Vienna ab initio simulation program (VASP). The ion-core interactions were represented by the projector–augmented wave (PAW) method. A plane wave basis set was used to expand the valence electron wave functions. The energy cutoff for the plane wave basis set was 520 eV A $(3 \times 3 \times 1)$ k-point sampling was used following the Monkhorst-Pack scheme, with the third vector perpendicular to the surface for all density functional theory (DFT) optimizations. The Perdew-Burke-Ernzerhof (PBE) version of the generalized gradient approximation (GGA) was used to include exchange and correlation energies. Structural optimizations were performed by minimizing the forces on all atoms to below 0.05 $eV{\cdot}Å^{-1}$.

The Ni catalyst is represented as a p(3 × 6) Ni(001) slab. The testing of thickness of nickel-layers in slab shows that the slab with three nickel-layers has similar electronic structure with the slab with five nickel-layers (shown in Fig. S1). Considering the CPU time and the accuracy of the calculation, the slab with three nickel-layers as the model is selected to do further study. The neighboring slabs are separated in the direction perpendicular to the surface by a vacuum region of 15 Å. As shown in Fig. 1a, the sign t, b and h represent the top, bridge and hollow adsorption sites on the Ni(001), respectively. The $(RuO_2)_4$ cluster (seen in Fig. 1e) is constructed according to ref. [37], in which Ru_4O_8 cluster has a C_{2v} geometry. The RuO_2/Ni(001) composite catalyst is shown in Fig. 1b, where I ~ V represent the Ni atoms at the RuO_2/Ni(001) interface, h©-I ~ h©-III represent the hollow adsorption sites close to the interface, h®-I represent the hollow adsorption sites far away from the interface, and t-Ru represents the top sites of Ru. To further verify the synergistic catalytic effect between metal oxide and metal for the HER, the NiO/Ni(001) with a p(3 × 6) slab (in Fig. 1c) and $(NiO)_2$/Ni(001) with a p(3 × 8) slab (in Fig. 1d) composite catalysts are also constructed. In addition, Pt(001) surface with a p(3 × 6) slab shown in Fig. 1g is used as a benchmark for indicating the activity of RuO_2/Ni(001), NiO/Ni(001), $(NiO)_2$/Ni(001) and Ni(001), where the h represents a hollow site on Pt. NiO(001) surface with a p(3 × 6) (Fig. 1f) supercell is also calculated to track the change of Ni atom from the metal to metal oxide, where b represents a bridge adsorption site on Ni.

The d-band center is calculated as the center of mass of the d-band overall energy values up to the Fermi energy. Unless otherwise stated, the d-band center is taken to be the average of the d-band center of the surface Ni atoms surrounding (or at) the adsorption sites under discussion. Transition states for H_2O dissociation, and H diffusion were located using the climbing image-nudged elastic band (CI-NEB) method [38], with six images placed between the reactant and product geometries. A -5.0 $eV{\cdot}Å^{-2}$ spring force constant between images is used to relax all of the images until the force acting on each atom is < 0.03 $eV{\cdot}Å^{-1}$. To ensure that the stationary structures were minimum energy structures (zero imaginary frequencies) or transition states (one imaginary frequency) and to calculate the zero-point energies (ZPE), vibrational frequency calculation [39] were performed using ionic displacements of 0.01 Å, and only the adsorbates were allowed to move.

The MD simulations of water/NiO/Ni(001) interfaces (model seen in SI) were performed using the LAMMPS MOLECULAR Dynamics Simulator [40] using periodic boundary conditions. The canonical (NVT) ensemble was employed by Nosé-Hoover thermostat method at a constant temperature of 300 K (SMASS ≥ 0). The simulations generated 2.0 ns of equilibrated trajectories with 0.5 fs as time step.

Adsorption energies are calculated according to

$$E_{ads} = E_{total} - E_{surface} - E_{adsorbates} \quad (1)$$

A negative value of E_{ads} corresponds to an energetically stable binding system.

The free energy change of H*, ΔG_{H^*} is calculated using Eq. (2):

$$\Delta G_{H^*} = HBE + \Delta E_{ZPE} - T\Delta S \quad (2)$$

Here, HBE (H* binding energy) can be calculated by taking the separated H_2 in a vacuum as a reference state [Eq. (3)]:

$$HBE = E_{(surface+H^*)} - E_{(surface)} - 1/2E_{H2} \quad (3)$$

We include corrections for the changes in the ZPE and entropy. According to the Sabatier principle, to obtain the maximum rate of the overall reaction, ΔG_{H^*} should be zero.

2.2. Catalyst synthesis

The fabrication of the NiO nanosheet catalysts was achieved via a two-step process. Firstly, a hydrothermal process was conducted to achieve a uniformly nanostructured Ni^{2+} precursor. Secondly, a heat-treated oxidation was applied to convert the Ni^{2+} precursors to NiO nanosheet. The NiO/Ni nanosheet catalysts with different NiO content were prepared by reducing the NiO nanosheet in a hydrogen atmosphere at different temperature for 1 h. When the reduction temperature increased to 400℃, the NiO nanosheet was totally reduced to Ni nanosheet. The reduced Ni nanosheet was immersed in an aqueous solution containing 0.073 mol L^{-1} $RuCl_3$, and then heated at 300℃ for 5 min in air to obtain the RuO_2/Ni nanosheet catalysts. The content of the RuO_2 was varied by the number of the immersion. A certain volume of the 20% Pt/C ink was carefully dropped onto the Ni substrate to obtain the Pt/C electrode with a desirable catalyst loading of 1.0 mg cm^{-2}. The samples reduced at different temperatures were named as NiO/Ni-x, for example, NiO/Ni-300 means NiO reduced at 300℃.

2.3. Characterization and electrochemical measurements

The surface morphology and the microstructure of the catalysts were analyzed by X-ray diffraction (XRD-6000, Shimadzu), X-ray photoelectron spectroscopy (XPS, ESCALAB 250Xi), and field-emission scanning electron microscopy (FE-SEM, JSM-7800, Japan). Electrochemical measurements were conducted in a three-electrode cell system using an Electrochemical Workstation (CHI660D, Shanghai Chenhua Device Company, China). Sizable and shapeable electrodes can be prepared by simply tailoring the Ni foam, and the obtained NiO/Ni can be directly used as the working electrode (1.0 cm^2) without

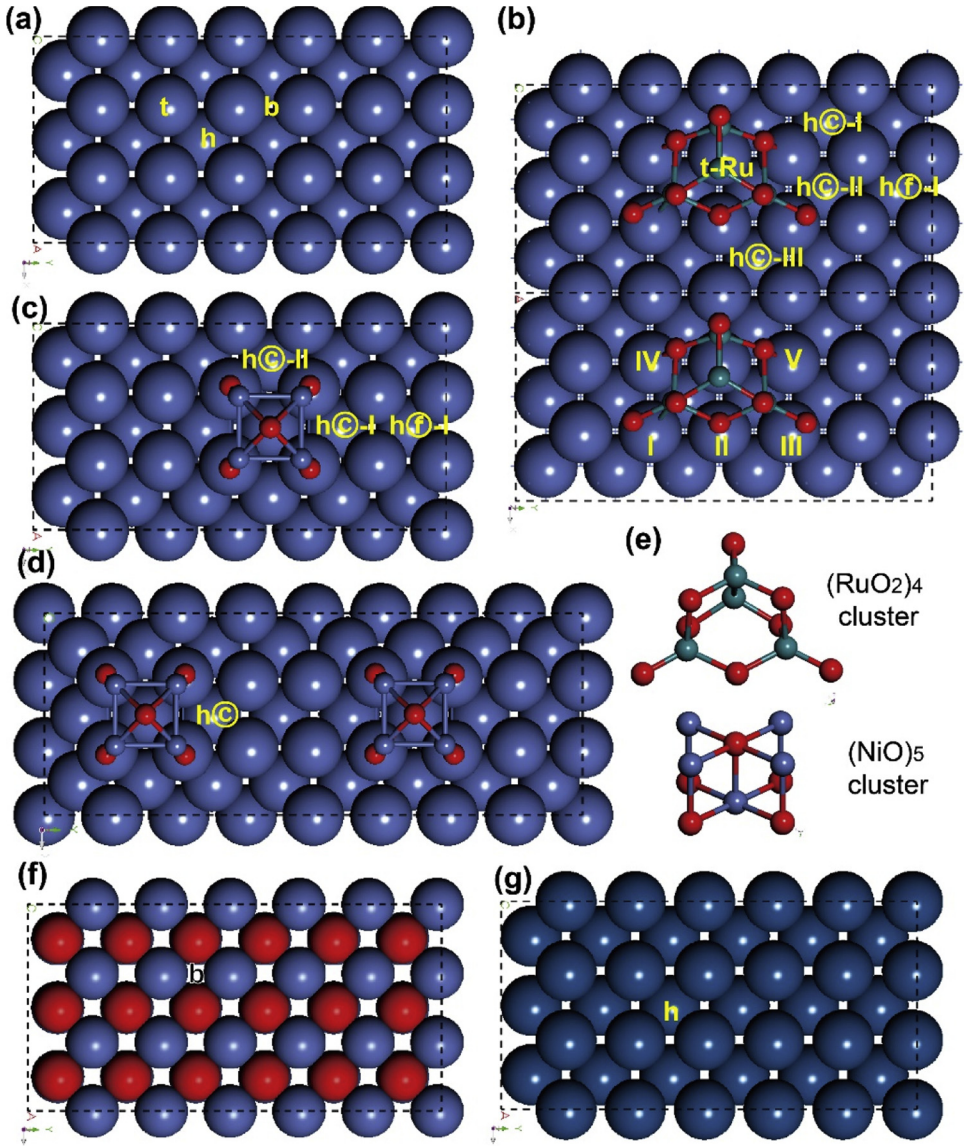

Fig. 1. Structure of (a) Ni (001), (b) RuO_2/Ni (001), (c) NiO/Ni(001), (d) $(NiO)_2$/Ni (001), (e) $(RuO_2)_4$, $(NiO)_5$ cluster, (f) NiO (001), and (g) Pt (001). Here, Ni, Pt, Ru and O atoms are shown in gray blue, dark blue, green and red, respectively. (For interpretation of the references to colour in this figure legend, the reader is referred to the web version of this article).

employing extra substrates (e.g., glassy-carbon electrode) or binders (e.g., Nafion). A carbon rod in parallel orientation to the working electrode with a distance of 1.0 cm was used as the counter electrode, and an Hg/HgO electrode was used as the reference electrode. Then, the catalytic performance of the prepared electrodes toward HER was systematically investigated in a 1.0 mol L^{-1} NaOH and 0.2 M PBS (pH = 7) electrolyte. The catalytic behaviors of different materials were studied and compared using LSV and CV at the scan rates of 10 mV/s and 50 mV/s, respectively. All potentials mentioned in this work were converted to values with reference to the reversible hydrogen electrode (RHE).

3. Results and discussion

3.1. Geometry and electronic structure

Firstly, we carried out systematic studies on the geometric structures and electronic properties of the RuO_2/Ni(001) catalyst using DFT calculations. Fig. 1 shows that the RuO_2 can be stably adsorbed on Ni (001) by five Ni-O (approximately 1.8 Å) and three Ni-Ru bonds (approximately 2.5 Å) with the adsorption energy of -5.7 eV, indicating a strong interaction between RuO_2 and Ni(001). The average Bader charge and the charge distribution confirm that the interaction between RuO_2 and Ni(001) is mainly contributed to by the interfacial Ni-O bonds. As illustrated in Fig. 2a and Table S1, Ni atoms and particularly the interfacial Ni atoms (marked as I ~ V) on RuO_2/Ni(001) carry more positive charge than the other Ni atoms on Ni(001), whereas the Ru atoms on RuO_2/Ni(001) have less positive charge than those on the bare RuO_2 cluster. The more positive charge of interfacial Ni atoms is mainly generated by the interfacial charge transfer from the Ni atoms to the O atoms in the RuO_2 cluster. The differential charge density of RuO_2/Ni(001) projected on the Ni(001) plane in Fig. 2b clearly shows the electron depletion on the I ~ V Ni atom sites. We note that the charge density accumulation around each of the I ~ V Ni atoms is attributed to the O atoms in RuO_2 that accept some of the electrons from the Ni atoms in the formation of the interfacial Ni-O bonds. In Fig. 2d, the charge density change between the O p-orbitals and Ni d-orbitals increases, indicating that the partial charges are transferred from Ni to O, and the interfacial Ni atoms are partially oxidized by O. Therefore, the interaction between the RuO_2 and Ni (001) is mainly caused by the

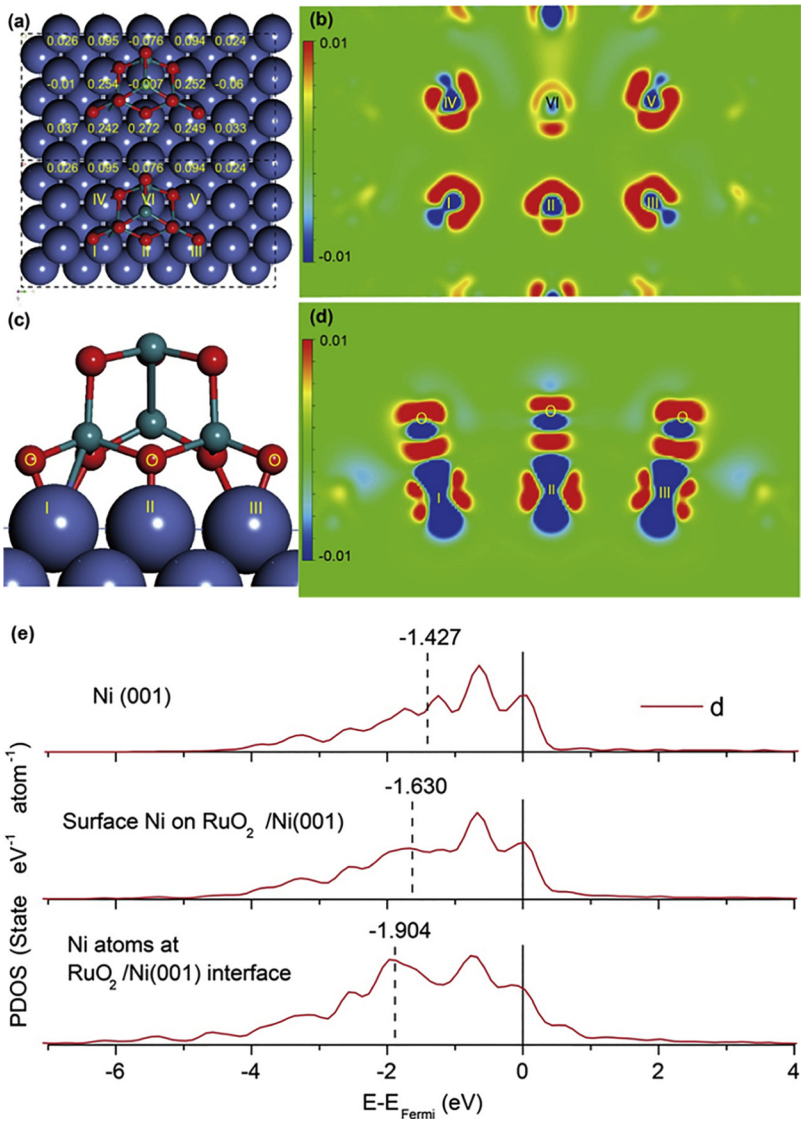

Fig. 2. (a) Bader charge distribution for surface Ni atoms on RuO_2/Ni (001). (b) differential charge density of RuO_2/Ni(001) projected on the (001) plane. (c) side view of RuO_2/Ni (001), and (d) differential charge density of RuO_2/Ni (001) projected on the side view. (e) partial density of states and d-band centre for Ni atoms on Ni (001) and RuO_2/Ni (001) surface.

Table 1
H_2O*, OH*, and H* adsorption energy on the Ni (001), RuO_2/Ni (001) and bare RuO_2 cluster.

Systems		Adsorption energy / E_{ads} (eV)		
		H_2O*	OH*	H*
Ni(001)		−0.288	−3.992	−3.983
RuO_2/Ni(001)	Ni sites at non-interface	−0.300	−3.961	−3.927
	Ni sites at interface	No adsorption	No adsorption	−3.687
	Ru sites	−0.472	−2.719	−3.852
Bare RuO_2 cluster		−0.781	−3.380	−3.151

interfacial charge transfer that increases the Bader charge of the interfacial Ni atoms.

In addition to the change in the charge distribution, the density of states and d-band center for Ni atoms (d-PDOS) on the Ni(001) and the RuO_2/Ni(001) also show distinct differences. Fig. 2e shows that for the three types of Ni atoms, the Ni atoms in Ni(001), the surface Ni atoms in RuO_2/Ni(001) and the interfacial Ni atoms in RuO_2/Ni(001), the d-band centers increasingly shift down away from the Fermi level. The interfacial Ni atoms (I ~ V) have the lowest d-band centers. The similar electronic structure also exists in the NiO/Ni (001) system (shown in Table S1). Generally, the d-band position has been used as a descriptor for the binding energy between the metal and adsorbates [41,42], that is, the lower the d-band center, the weaker the binding energy. Thus, such interfacial Ni atoms should have the weakest interaction with adsorbates such as H, OH, and H_2O, compared with the non-interfacial Ni atoms and Ni(001).

3.2. Determination of the synergistically enhanced active sites

To determine the synergistically enhanced active sites for the HER on the RuO_2/Ni(001) surface, we investigated the H_2O*, OH* and H* adsorption behaviour on Ni (001), RuO_2/Ni(001) and the bare RuO_2 cluster. Table 1 shows the most stable adsorption energy of H*, H_2O* and OH*. On the Ni surface, H_2O* and OH* prefer to be adsorbed on the bridge site, whereas H* is prone to adsorb on the 4-fold hollow site. On the RuO_2, the most stable adsorption site for H_2O*, OH* and H* is the Ru top site. The screening of H_2O* and OH* stable adsorption sites on the RuO_2/Ni(001) found that H_2O* and OH* cannot adsorb on the interfacial Ni atoms due to the strong repulsion from the metal oxide

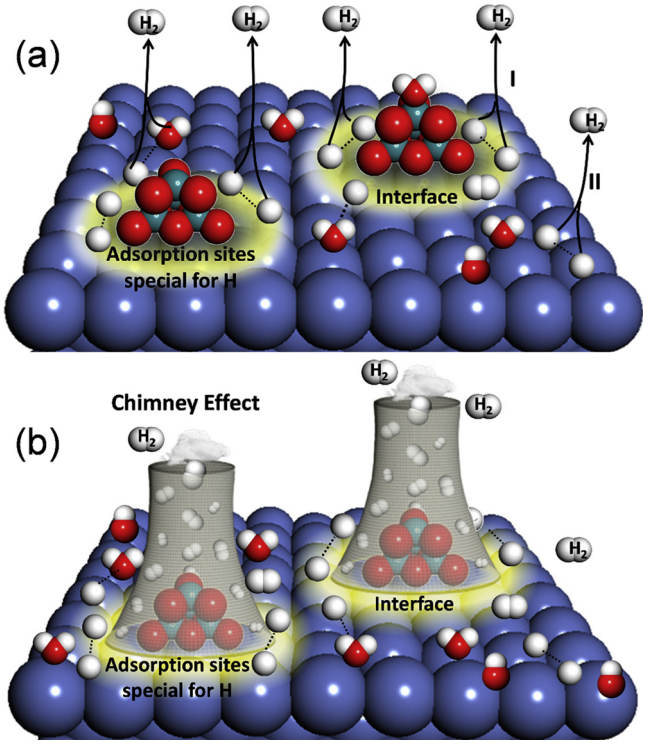

Scheme 1. Schematic diagrams of the proposed HER mechanism on the RuO_2/Ni composite catalysts. (a) Two possible HER pathway, (b) a "Chimney Effect" at the interface.

cluster, while H has stable adsorption on the interfacial Ni atoms and the non-interfacial Ni atoms. And the interfacial Ni atoms has slight weaker interaction with H* than non-interfacial Ni sites. On NiO/Ni (001) surface, the H*, H_2O* and OH* also exhibit similar adsorption behaviours as shown in Table S2. The water radial distribution functions (RDF) on NiO/Ni(001) surface (Fig. S3) resulting from the MD simulation further prove that the interfacial Ni atoms have more loosely bound (2.95 Å) with water molecules than non-interfacial Ni atoms (2.25 Å). On the contrary, the too strong adsorption of H*, and the competitive adsorption among H_2O*, OH* and H* on non-interfacial Ni atoms, can hinder the adsorption/desorption efficiency of H*. Thus, the interfacial Ni atoms exhibit a high selectivity for H* adsorption compared with the non-interfacial Ni atoms. Combined with the changes in electronic structure, we speculate that the interfacial Ni atoms in metal oxide/metal are the synergistically enhanced active sites, and play a role of an easy channel for hydrogen evolution due to the favourable adsorption/desorption of H*, which can set up an efficient chimney for hydrogen evolution along the interface of metal oxide/metal as shown in Scheme 1.

In addition, the H_2O* and OH* adsorption energies on the non-interfacial Ni atoms in RuO_2/Ni(001) are similar to those on Ni(001), whereas the H_2O* and OH* adsorption energies on Ru sites in RuO_2/Ni (001) become weaker than those on the bare RuO_2 cluster. Transition state calculations show that the activation energies (E_a) of H_2O dissociation on the Ni(001) and the non-interfacial Ni atoms in RuO_2/Ni (001) are very close and are approximately 0.32 eV and 0.40 eV, respectively (see in Fig. S4). This means that the combination of RuO_2 and Ni do not improve the dissociation of water on the non-interfacial Ni sites. Then, the interface-induced synergistic effect of metal oxide/metal composites on HER can hardly be attributed to the splitting of H_2O or the adsorption of OH; therefore, H adsorption/desorption might be the critical step.

3.3. Analysis of the enhanced HER activity

Based on the difference between interface and non-interface on the metal oxide/metal, as shown in Scheme 1, we speculate that there are two possible HER pathways on the metal oxide/metal composite catalyst, with one occurring on the sites close to the interface (ⓒ) and another involving reaction on the sites far away from the interface (ⓕ). First, the adsorbed H_2O* on the metal or metal oxide (MO) is dissociated to OH* and H*. The generated H* may then adsorb on the sites close to the interface or far away from the interface. Subsequently, these two different adsorption sites of H* may induce different mechanisms and catalytic behavior towards HER, thus affecting the final activity.

Before we explore a deep insight into the above point, let us discuss an important descriptor for the HER in advance. The H adsorption free energy (ΔG_{H^*}) that has been considered to be the major descriptor of the HER activity for a wide variety of metal surfaces [6,39]. Because the Ni atoms regardless of from the Ni(001) or from the RuO_2/Ni(001) have the same capability to dissociate the water, thus, the HER activity on RuO_2/Ni(001) and Ni(001) can be predicted by the ΔG_{H^*}. The optimal value of $|\Delta G_{H^*}|$ should be close to zero; too positive and too negative ΔG_{H^*} corresponding to the difficult formation and desorption of H* respectively, means the sluggish kineties of HER.

The examination of the HER free energy values listed in Fig. 3a shows that Ni(001) exhibits a highly negative ΔG_{H^*} value, indicating a relatively strong HBE; in sharp contrast, metal oxides, such as NiO(001) and bare RuO_2 cluster display highly positive ΔG_{H^*} values, corresponding to a too weak HBE. For RuO_2/Ni(001), regardless of the reaction site, the ΔG_{H^*} values are all negative and shift to the zero direction relative to that on Ni(001). Among all reaction sites on the RuO_2/Ni(001) surface, the ΔG_{H^*} at the sites close to the interface are much closer to zero than those at the sites far away from the interface. The ΔG_{H^*} values of RuO_2/Ni-hⓒ-II and RuO_2/Ni-hⓒ-III are particularly close to that of Pt(001), indicating the most favorable H* adsorption/desorption property and HER activity comparable to that of Pt. The results are consistent with our previous experimental work [16], in which the RuO_2/Ni composite catalyst with only 5.7 at% Ru displays an enhanced HER catalytic activity compared with a Pt catalyst in a 6 mol L^{-1} NaOH solution. The above observation is also shown to be true for other metal-oxide/metal system such as NiO/Ni, as shown in Figs. 3b and Fig. S6. It suggests that it is possible to enhance the HER enabling the use of cheap metal oxides as substitutes for noble metal oxides.

Based upon the above results, we propose the following two mechanisms of the HER at two types of Ni sites shown in Scheme 1a :

Path I (at the sites close to the interface):

$$H_2O^*ⓕ + e^- \rightarrow OH^-ⓕ + H^*ⓒ \quad \text{(I-1.1)}$$

$$H_2O^*(MO) + e^- \rightarrow OH^-(MO) + H^*ⓒ \quad \text{(I-1.2)}$$

$$H^*ⓒ + H_2O^*ⓕ + e^- \rightarrow OH^-ⓕ + H_2 \quad \text{(I- 2.1)}$$

$$H^*ⓒ + H_2O^*(MO) + e^- \rightarrow OH^-(MO) + H_2 \quad \text{(I-2.2)}$$

$$2H^*ⓒ \rightarrow H_2 \quad \text{(I-3)}$$

Path II (at the sites far away from the interface):

$$H_2O^*ⓕ + e^- \rightarrow OH^-ⓕ + H^*ⓕ \quad \text{(II-1)}$$

$$H^*ⓕ + H_2O^*ⓕ + e^- \rightarrow OH^-ⓕ + H_2 \quad \text{(II-(2)}$$

$$2H^*ⓕ \rightarrow H_2 \quad \text{(II-3)}$$

On the sites close to the interface, the adsorbed H* is generated from the dissociation of H_2O* on metal oxide and on non-interface Ni atoms. While the adsorbed H* on the sites far away from the interface only can be produced from the non-interface Ni atoms. It indicates that the more H* can transfer to the sites close to the interface than the sites far away from the interface. More important, because the interfacial Ni atoms in

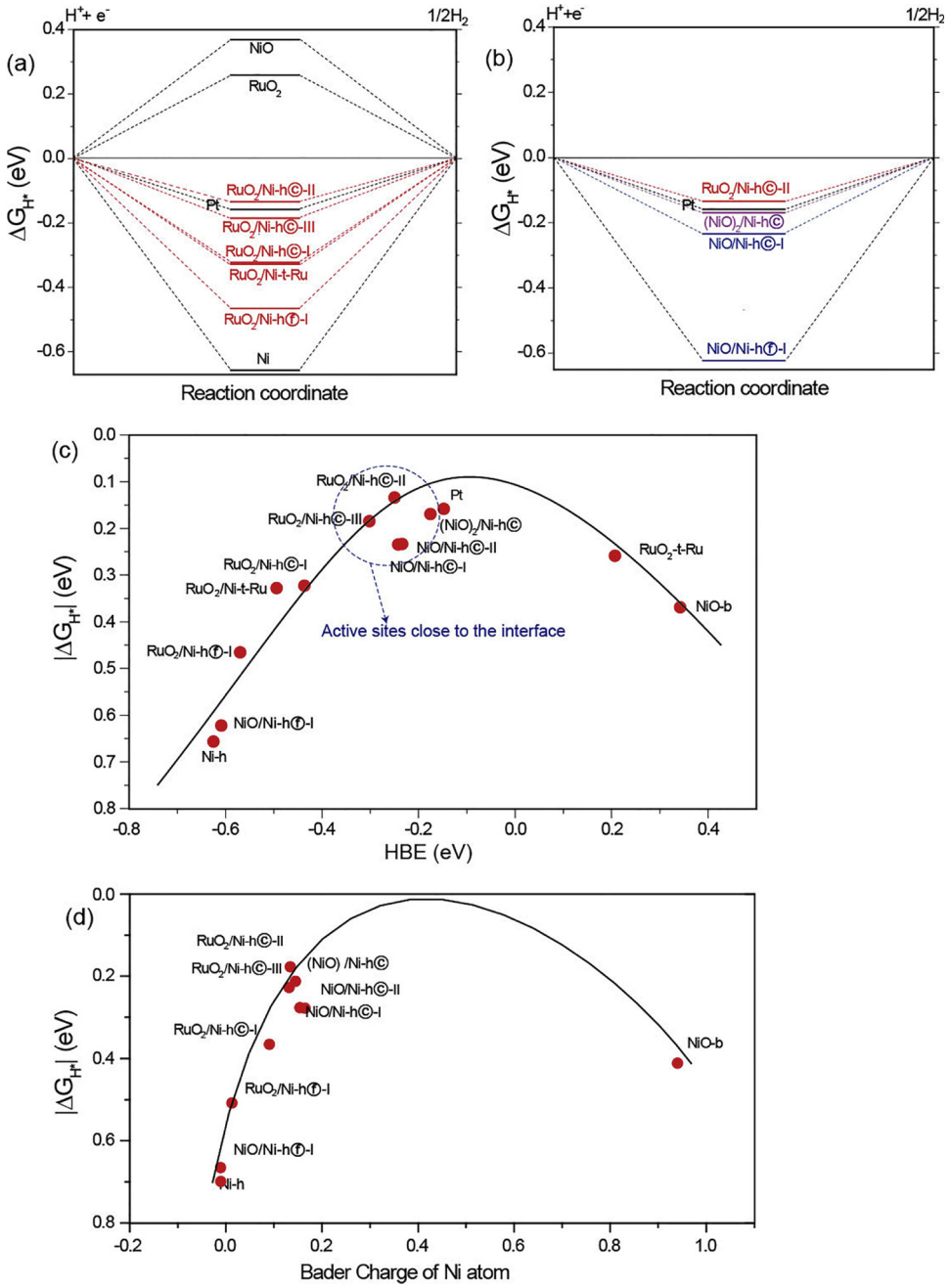

Fig. 3. Calculated free energy (ΔG_{H^*}) diagram for HER at the equilibrium potential (U_{RHE} = 0 V) for (a) Ni (001), Pt (001), NiO (001), RuO_2 cluster and RuO_2/Ni (001), and for (b) NiO/Ni (001) and $(NiO)_2$/Ni(001). (c) the relationship between ΔG_{H^*} and HBE for various adsorption sites in catalysts. (d) the relationship between ΔG_{H^*} and Bader charge of Ni atoms in catalysts.

metal oxide/Ni(001) have a more favorable H* adsorption/desorption property than the non-interfacial Ni atoms and adsorb the H* selectively, the combination of H* and desorption of H_2, that is, reactions I-2.1, I-2.2, and I-3 are thus much preferred than the reactions II-2, and II-3. Then, a hydrogen evolution chimney will be formed along the metal oxide/Ni(001) interface as shown in Scheme 1b. This means that, besides the metal oxide, the interface between the metal oxide and metal as the interface-induced optimal active sites promotes a favorable adsorption of reactant (H*) and an easy desorption of the product (H_2). A favorable desorption rate of H_2 on the sites around the interface would release more free sites, making the adsorption of H* on the active sites easier and smoother, and then form a hydrogen evolution chimney around the interface that acts as the main channel for hydrogen evolution over the entire surface of the metal-oxide/metal system. Accordingly, their number of such chimneys for hydrogen evolution will increase with the number of such metal-oxide/metal interfaces increasing.

Fig. 3c presents the relationship between ΔG_{H^*} and HBE. It can be observed that the sites close to the interface in the metal oxide/metal composite catalysts have a more proper HBE, leading the $|\Delta G_{H^*}|$ value to be located on the top of the volcano. The relationship between ΔG_{H^*} and HBE implies that the HER activity of a metal oxide/metal composite catalyst depends strongly on the distance of sites from the interface and can be modulated by adjusting the oxidation state and coverage of the metal oxide.

The influence of oxidation state and coverage of the metal oxide on the HER activity of metal oxide/metal composite catalysts can be tracked by the Bader charge of the interfacial Ni atom. As shown in

Fig. 3d, the Ni sites close to the interface in RuO_2/Ni(001) and NiO/Ni (001), where Ni atoms show a charge value located between that of Ni (001) and NiO(001), exhibit the highest HER activity (the $|\Delta G_{H^*}|$ value close to zero). This reveals that the charge of the metal atom should be another important and convenient descriptor for indicating the activity of the metal/metal oxide composite catalysts. Then, the HER activity of metal oxide/metal composite catalysts can be enhanced by modulating the interface charge transfer of the metal oxide/metal systems. No doubt, metal oxide with high oxidation state such as RuO_2 can reach the top of the volcano at a relative low coverage. Whereas the metal oxide with low oxidation state, such as NiO, should increase its coverage on the metal to approach the top of the volcano. However, too high coverage of metal oxide might decrease the number of metal oxide/metal interface due to the agglomeration among the metal oxide particles, leading to a reduction of the chimney amount, i.e., the number of the interface-induced synergistically enhanced active sites. Thus, the loading of metal oxide with low oxidation state should take account of interface charge transfer effect and the amount of the metal oxide/metal interfaces.

To validate the conclusion of the theoretical calculations described above, a series of NiO/Ni nanosheet composite catalysts with different amounts of the interface were fabricated by varying the NiO contents. Fig. S7a-c shows the SEM images and the EDX mapping of the NiO/Ni nanosheet reduced in hydrogen atmosphere at different temperatures, revealing that the O contents are decreasing with the reduced temperature. The XRD patterns given in Fig. 4a show that the intensity of Ni peak increases and the intensity of NiO peak decreases by raising the reduction temperature from 240 to 400℃, indicating the NiO content in NiO/Ni catalysts gradually decreases with increasing reduction temperature. The NiO were totally converted to Ni as reduction temperature reached 400℃. Compared with the metallic Ni, the Ni (111) facets (figure insert in Fig. 4a) of the other samples shift to the low degree with increasing NiO content. The peak shift of Ni(111) can be attributed to the changed crystal structure of Ni affected by NiO content. XPS data shown in Fig. 4b, Figs. S8-9 and Table S3 also confirm the interaction between NiO and Ni phase. As shown in Fig. 4b, the Ni $2p_{3/2}$ peak of NiO/Ni-300 can be divided into five peaks. The peak at 852.6 and 861.9 eV are characteristic of Ni° in Ni metal (Ni_{Ni}), and the peaks at 854.4 and 856.4 eV are indexed to the NiO (Ni_{NiO}). Interestingly, the binding energy of Ni $2p_{3/2}$ appears a new peak at 855.3 eV, which can be indexed to the interfacial Ni ($Ni_{interface}$) due to the charge transfer between NiO and Ni phase. Comparing the Ni XPS spectra of all the six samples (seen in Figs. S8-9 and Table.S3), the changes of the peak of Ni_{NiO}, O and Ni_{Ni} in NiO/Ni catalysts surface further confirm that the content of NiO relative to Ni can be decreased continuously by increasing the reduction temperature. Most important, from the NiO to the Ni, the atomic content of the $Ni_{interface}$ (shown in Table S4) in these samples firstly increases and then decreases gradually, in which, NiO/Ni-300 shows the largest $Ni_{interfacae}$ atomic content of 28.06%. It confirms that the amount of the NiO/Ni interfaces can be tuned effectively by changing the NiO content.

To probe the catalytic activity of NiO/Ni catalysts, we conducted the HER performance tests for all samples in 1 M NaOH and 0.2 M PBS solution respectively (Figs. S10 and S11). LSV curves described in Fig. 4c suggest that all the NiO/Ni catalysts display higher HER activity than the pure NiO and Ni catalysts. Similar HER activity trend of catalysts also can be found in PBS solution. From NiO/Ni-240 to NiO/Ni-350 catalysts, the HER activity of samples firstly increases with the increase of reduction temperature, and then decreases gradually. Among various NiO/Ni samples, the NiO/Ni-300 catalyst exhibits the best catalytic activity, reaching a current density of 10 $mA{\cdot}cm^{-2}$ at a low overpotential of 194 mV in 1 M NaOH solution. Nyquist plots obtained by EIS measurement (Figs. S10b, and S11b) indicate that the NiO/Ni-300 has the lowest charge transfer resistance in all NiO/Ni catalysts. Besides, it should be noted that all prepared NiO/Ni catalysts have almost the same active specific surface areas (seen in Table S5) and similar Tafel slop (Fig. S12), which avoid the influence of the number of active sites and HER pathways on the comparison of catalysts' activity. As shown in Fig. 4d, the change of the HER activity of NiO/Ni samples is in agreement with the variation tendency of $Ni_{interface}$ atomic content, implying a strong correlation between the HER activity and the amount of NiO/Ni interface. Firstly, with increase of the reduction temperature, the NiO gradually convert into the Ni phase, and the NiO/Ni interfaces are appeared, consequently enhancing the catalytic activity of NiO/Ni. The NiO/Ni interface content reaches a maximum value (28.06%) at the optimal reduction temperature of 300℃, which results in the best catalytic activity of NiO/Ni among the various NiO/Ni samples. Further increasing the reduction temperature would excessively decrease the NiO contents, and lead to a reduction of the NiO/Ni interface content, finally cause the catalytic activity of NiO/Ni to drop down. The larger content of the interface between metal oxides and metals means more chimneys are formed along the interface,

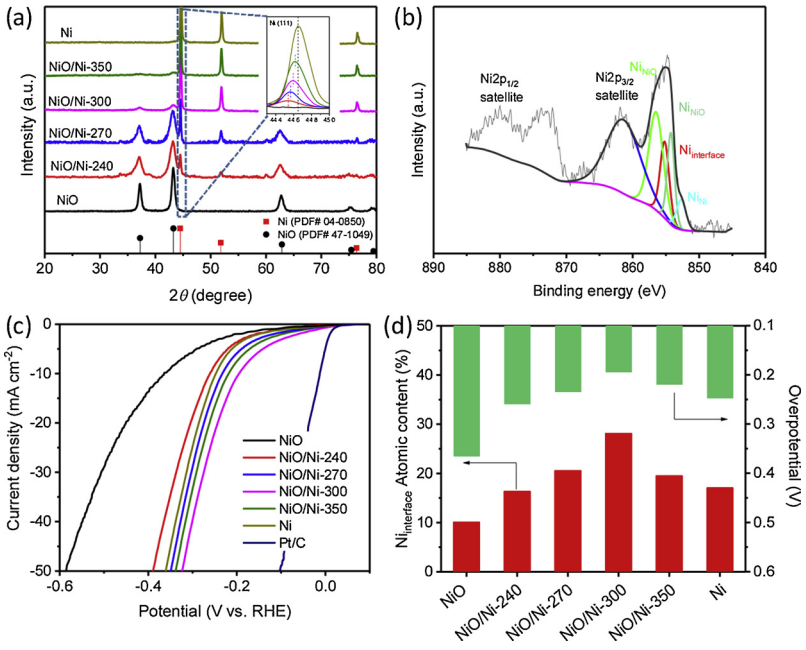

Fig. 4. (a) XRD patterns of Ni, NiO and NiO/Ni catalysts with different NiO contents varying with reduction temperature. (b) Ni 2p XPS spectrum of NiO/Ni-300. (c) HER current density on Ni carrying different amounts of NiO in a 1.0 mol L^{-1} NaOH electrolyte at a sweep rate of 10 mV s^{-1}. (d) Comparisons of the content of $Ni_{interface}$ specie on the surfaces of the prepared samples and their activities.

and more efficient HER can be expected on such metal oxides/metals systems. Therefore, the results from the experimental validate that the "chimney effect" should be the original of the interface-induce synergistic effect on the metal oxide/metal composite catalysts for catalysing HER.

4. Conclusions

In summary, based on the DFT-calculation and experiment results, we propose a "chimney effect" for the HER on the interface between the metal oxide/metal catalysts. It reveals a new side of the nature of the interface-induced synergistic effect of metal oxide/metal composite catalysts. Firstly, the interface of metal oxide/Ni (001) is immune to OH* and H_2O* adsorption, but is available for only H* adsorption. Secondly, the interface between the metal oxide and the metal as the optimal active site allows a favorable adsorption of the reactant (H*), and an easy desorption of the product (H_2), thus, an easy channel along the interface for the HER is formed. Thirdly, the efficiency of such a hydrogen evolution chimney, which is highly related to the values of ΔG_{H^*}, can be tuned by modulating the loading, distribution and types of metal oxide. Finally, the "chimney effect" is a result of the interfacial charge transfer from the metal oxide to metal; then, the charge state of the interfacial metal atoms can be another important and convenient descriptor for indicating the activity trends.

Conflicts of interest

There are no conflicts to declare.

Acknowledgements

This work was financially supported by National Natural Science Foundation of China (Grants 21576032, 21436003, and 91535205).

Appendix A. Supplementary data

Supplementary material related to this article can be found, in the online version, at doi:https://doi.org/10.1016/j.apcatb.2018.12.035.

References

[1] H.J. Lv, W.W. Guo, K.F. Wu, Z.Y. Chen, J. Bacsa, D.G. Musaev, Y.V. Geletii, S.M. Lauinger, T. Lian, C.L. Hill, A. Noble-Metal-Free, Tetra-nickel polyoxotungstate catalyst for efficient photocatalytic hydrogen evolution, J. Am. Chem. Soc. 136 (2014) 14015–14018.
[2] L. Liao, S.N. Wang, J.J. Xiao, X.J. Bian, Y.H. Zhang, M.D. Scanlon, X.L. Hu, Y. Tang, B.H. Liu, H.H. Girault, A nanoporous molybdenum carbide nanowire as an electrocatalyst for hydrogen evolution reaction, Energy Environ. Sci. 7 (2014) 387–392.
[3] Q. Liu, J.Q. Tian, W. Cui, P. Jiang, N.Y. Cheng, A.M. Asiri, X.P. Sun, Carbon nanotubes decorated with CoP nanocrystals: a highly active non-noble-Metal nanohybrid electrocatalyst for hydrogen evolution, Angew. Chem. Int. Ed. 53 (2014) 6710–6714.
[4] K. Kitamoto, K. Sakai, Pigment- acceptor- catalyst triads for photochemical hydrogen evolution, Angew. Chem. Int. Ed. 53 (2014) 4618–4622.
[5] L. Cheng, W.J. Huang, Q.F. Gong, C.H. Liu, Z. Liu, Y.G. Li, H.J. Dai, Ultrathin WS2 nanoflakes as a high-performance electrocatalyst for the hydrogen evolution reaction, Angew. Chem. Int. Ed. 53 (2014) 7860–7863.
[6] Y. Zheng, Y. Jiao, M. Jaroniec, S.Z. Qiao, Advancing the electrochemistry of the hydrogen-evolution reaction through combining experiment and theory, Angew. Chem. Int. Ed. 54 (2015) 52–65.
[7] S.E. Fosdick, S.P. Berglund, C.B. Mullins, R.M. Crooks, Evaluating electrocatalysts for the hydrogen evolution reaction using bipolar electrode arrays: Bi- and trimetallic combinations of Co, Fe, Ni, Mo, and W, ACS Catal. 4 (2014) 1332–1339.
[8] C.B. Liu, L.L. Wang, Y.H. Tang, S.L. Luo, Y.T. Liu, S.Q. Zhang, Y.X. Zeng, Y.Z. Xu, Vertical single or few-layer MoS2 nanosheets rooting into TiO2 nanofibers for highly efficient photocatalytic hydrogen evolution, Appl. Catal. B Environ. 164 (2015) 1–9.
[9] X. Ji, B. Liu, X. Ren, X. Shi, A.M. Asiri, X. Sun, P-doped Ag nanoparticles embedded in N-Doped carbon nanoflake: an efficient electrocatalyst for the hydrogen evolution reaction, ACS Sustain. Chem. Eng. 6 (2018).
[10] Y. Ji, L. Yang, X. Ren, G. Cui, X. Xiong, X. Sun, Nanoporous CoP3 nanowire array: acid etching preparation and application as a highly active electrocatalyst for the hydrogen evolution reaction in alkaline solution, ACS Sustain. Chem. Eng. 6 (2018) 11186–11189.
[11] J. Tian, Q. Liu, A.M. Asiri, X. Sun, Self-supported nanoporous cobalt phosphide nanowire arrays: an efficient 3D hydrogen-evolving cathode over the wide range of pH 0-14, J. Am. Chem. Soc. 136 (2014) 7587–7590.
[12] X. Han, Y. Yu, Y. Huang, D. Liu, B. Zhang, Photogenerated carriers boost water splitting activity over transition Metal/Semiconducting metal oxide bifunctional electrocatalysts, ACS Catal. 7 (2017).
[13] Z. Sun, Y. Liang, Y. Wu, Y. Yu, B. Zhang, Boosting electrocatalytic hydrogen-evolving activity of Co/CoO heterostructured nanosheets via coupling photogenerated carriers with photothermy, ACS Sustain. Chem. Eng. 6 (2018) 11206–11210.
[14] J. Tian, N. Cheng, Q. Liu, X. Sun, Y. He, A.M. Asiri, Self-supported NiMo hollow nanorod array: an efficient 3D bifunctional catalytic electrode for overall water splitting, J. Mater. Chem. A 3 (2015) 20056–20059.
[15] Z. Wang, X. Ren, Y. Luo, L. Wang, G. Cui, F. Xie, H. Wang, Y. Xie, X. Sun, An ultrafine platinum-cobalt alloy decorated cobalt nanowire array with superb activity toward alkaline hydrogen evolution, Nanoscale 10 (2018) 12302–12307.
[16] K. Xiong, L. Li, Z. Deng, M. Xia, S. Chen, S. Tan, X. Peng, C. Duan, Z. Wei, RuO2 loaded into porous Ni as a synergistic catalyst for hydrogen production, RSC Adv. 4 (2014) 20521.
[17] W. Cui, Q. Liu, Z.C. Xing, A.M. Asiri, K.A. Alamry, X. Sun, MoP nanosheets supported on biomass-derived carbon flake: one-step facile preparation and application as a novel high-active electrocatalyst toward hydrogen evolution reaction, Appl. Catal. B Environ. 164 (2015) 144–150.
[18] S.K. Kim, Y. Qiu, Y.-J. Zhang, R. Hurt, A. Peterson, Nanocomposites of transition-metal carbides on reduced graphite oxide as catalysts for the hydrogen evolution reaction, Appl. Catal. B Environ. 235 (2018) 36–44.
[19] R. Subbaraman, D. Tripkovic, D. Strmcnik, K.-C. Chang, M. Uchimura, A.P. Paulikas, V. Stamenkovic, N.M. Markovic, Enhancing hydrogen evolution activity in water splitting by tailoring Li+-Ni(OH)2-Pt interfaces, Science 334 (2011) 1256–1260.
[20] D. Strmcnik, M. Uchimura, C. Wang, R. Subbaraman, N. Danilovic, V. van der, A.P. Paulikas, V.R. Stamenkovic, N.M. Markovic, Improving the hydrogen oxidation reaction rate by promotion of hydroxyl adsorption, Nat. Chem. 5 (2013) 300–306.
[21] Y. Liang, Y. Li, H. Wang, H. Dai, Strongly coupled inorganic/nanocarbon hybrid materials for advanced electrocatalysis, J. Am. Chem. Soc. 135 (2013) 2013–2036.
[22] J. Shi, On the synergetic catalytic effect in heterogeneous nanocomposite catalysts, Chem. Rev. 113 (2013) 2139–2181.
[23] H.Y. Kim, G. Henkelman, CO oxidation at the interface between doped CeO2 and supported Au nanoclusters, J. Phys. Chem. Lett. 3 (2012) 2194–2199.
[24] M. Fronzi, S. Cereda, Y. Tateyama, A. De Vita, E. Traversa, Ab initio investigation of defect formation at ZrO2-CeO2 interfaces, Phys. Rev. B 86 (2012) 085407.
[25] Y. Yu, Y. Shi, B. Zhang, Synergetic transformation of solid inorganic-organic hybrids into advanced nanomaterials for catalytic water splitting, Acc. Chem. Res. 51 (2018) 1711–1721.
[26] R. Subbaraman, D. Tripkovic, K.-C. Chang, D. Strmcnik, A.P. Paulikas, P. Hirunsit, M. Chan, J. Greeley, V. Stamenkovic, N.M. Markovic, Trends in activity for the water electrolyser reactions on 3d M(Ni,Co,Fe,Mn) hydr(oxy)oxide catalysts, Nat. Mater. 11 (2012) 550–557.
[27] J. Durst, A. Siebel, C. Simon, F. Hasché, J. Herranz, H.A. Gasteiger, New insights into the electrochemical hydrogen oxidation and evolution reaction mechanism, Energy Environ. Sci. 7 (2014) 2255–2260.
[28] W. Sheng, Z. Zhuang, M. Gao, J. Zheng, J.G. Chen, Y. Yan, Correlating hydrogen oxidation and evolution activity on platinum at different pH with measured hydrogen binding energy, Nat. Commun. 6 (2015).
[29] W. Sheng, M. Myint, J.G. Chen, Y. Yan, Correlating the hydrogen evolution reaction activity in alkaline electrolytes with the hydrogen binding energy on monometallic surfaces, Energy Environ. Sci. 6 (2013) 1509.
[30] J. Zhang, T. Wang, D. Pohl, B. Rellinghaus, R. Dong, S. Liu, X. Zhuang, X. Feng, Interface engineering of MoS2 /Ni3 S2 heterostructures for highly enhanced electrochemical overall-water-Splitting activity, Angew. Chem. Int. Ed. 55 (2016) 6702–6707.
[31] Z. Weng, W. Liu, L.C. Yin, R. Fang, M. Li, E.I. Altman, Q. Fan, F. Li, H.M. Cheng, H. Wang, Metal/Oxide interface nanostructures generated by surface segregation for electrocatalysis, Nano Lett. 15 (2015) 7704.
[32] X. Long, H. Lin, D. Zhou, Y. An, S. Yang, Enhancing full water-splitting performance of transition metal bifunctional electrocatalysts in alkaline solutions by tailoring CeO2–Transition metal oxides–Ni nanointerfaces, ACS Energy Lett. 3 (2018).
[33] W. Jing, S. Mao, Z. Liu, Z. Wei, H. Wang, Y. Chen, W. Yong, Dominating role of Ni0 on the interface of Ni/NiO for enhanced hydrogen evolution reaction, ACS Appl. Mater. Interfaces 9 (2017) 7139.
[34] B. He, Y. Kuang, Z. Hou, M. Zhou, X. Chen, Enhanced electrocatalytic hydrogen evolution activity of nickel foam by low-temperature-oxidation, J. Mater. Res. 33 (2018) 1–12.
[35] M. Gong, W. Zhou, M.C. Tsai, J. Zhou, M. Guan, M.C. Lin, B. Zhang, Y. Hu, D.Y. Wang, J. Yang, Nanoscale nickel oxide/nickel heterostructures for active hydrogen evolution electrocatalysis, Nat. Commun. 5 (2013) 4695.
[36] X. Zheng, L. Peng, L. Li, N. Yang, Y. Yang, J. Li, J. Wang, Z. Wei, Role of non-metallic atoms in enhancing the catalytic activity of nickel-based compounds for hydrogen evolution reaction, Chem. Sci. 9 (2018) 1822.
[37] H. Dong, L. Zhang, X. Zhou, Theoretical investigation on RuO2 nanoclusters adsorbed on TiO2 rutile (110) and anatase (101) surfaces, Theor. Chem. Acc. 133 (2014) 1–9.
[38] Y. Zheng, Y. Jiao, Y. Zhu, L.H. Li, Y. Han, Y. Chen, A. Du, M. Jaroniec, S.Z. Qiao, Hydrogen evolution by a metal-free electrocatalyst, Nat. Commun. 5 (2014).
[39] B. Hinnemann, P.G. Moses, J. Bonde, K.P. Jørgensen, J.H. Nielsen, S. Horch, I. Chorkendorff, J.K. Nørskov, Biomimetic hydrogen evolution: MoS2 nanoparticles as catalyst for hydrogen evolution, J. Am. Chem. Soc. 127 (2005) 5308–5309.
[40] S. Plimpton, Fast Parallel Algorithms for Short-range Molecular Dynamics, Academic Press Professional, Inc., 1995.
[41] M.T.M. Koper, H.A. Heering, Comparison of Electrocatalysis and Bioelectrocatalysis of Hydrogen and Oxygen Redox Reactions, Fuel Cell Science, John Wiley & Sons, Inc., 2010, pp. 71–110.
[42] J.K. Norskov, T. Bligaard, J. Rossmeisl, C.H. Christensen, Towards the computational design of solid catalysts, Nat. Chem. 1 (2009) 37–46.